

Short Communication

# Preparation and Electrochemical Study of Ag Nanoparticles Decorated on Gallium Arsenide as Photocatalyst for Methyl Orange Degradation Under Visible Light

Yuan Xu<sup>1,2</sup>, Yun-Sheng Qian<sup>1,\*</sup>, Jian-Liang Qiao<sup>2</sup>, Da-Yong Huang<sup>2</sup>, Shao-Bo Cui<sup>2</sup>

<sup>1</sup> School of Electronic and Optical Engineering, Nanjing University of Science & Technology, Nanjing, 210094, China

<sup>2</sup> School of Information Engineering, Nanyang Institute of Technology, Nanyang, 473004, China

\*E-mail: [qian\\_science@sina.com](mailto:qian_science@sina.com)

Received: 4 October 2021 / Accepted: 2 November 2021 / Published: 5 January 2022

---

The purpose of this research was to investigate the electrochemical growth of Ag nanoparticles on a gallium arsenide (GaAs) electrode and their use as photocatalysts for the degradation of methyl orange (MO) dyes under UV and visible irradiation. SEM and XRD were used to study the morphology and structure of the produced electrodes, revealing that Ag NPs in fcc structures were electrodeposited uniformly on the GaAs electrode surface. According to the optical studies, the optical band-gap values for nanostructured GaAs and Ag NPs/GaAs films were 2.23 eV and 2.16 eV, respectively. According to EIS analysis, the Ag NPs/GaAs film had a decreased photo-excited carrier recombination rate due to the effective separation of photo-induced electron-hole pairs. MO photodegradation experiments demonstrate that under UV and visible radiation, complete elimination of MO takes 46 and 40 minutes, respectively. As a result of lowering optical band-gaps, photocatalytic activity on Ag NPs/GaAs photocatalyst was significantly enhanced under visible light.

---

**Keywords:** Ag NPs/gallium arsenide; Photodegradation; Electrodeposition method; Methyl orange

## 1. INTRODUCTION

The industrialization has brought numerous benefits to human existence, including advancements in medicine, improved communication, increased agricultural efficiency, and economic prosperity [1]. However, industrialization has a number of drawbacks, including threats to plant life, global warming, deforestation, climate change, and pollutions, soil, and water, which results in the extermination of so many plants and animals, as well as respiratory problems, forms of cancer, and harm to antenatal care [2, 3]. As a result, numerous studies have focused on water reclamation and

reuse, which provide a unique and feasible way to supplement traditional water supply [4]. Organic dyes are a type of pollution produced by printing, photographing, painting, leather, and textile manufacturing effluent [5].

In the textile, culinary, and pharmaceutical sectors, methyl orange is among the most often used azo dyes [6, 7]. It has been revealed in studies that it can be used to identify hydrogen gas and hydrochlorides. It's also renowned for being a pH indicator. As a result, methyl orange application and introduction might have a major impact on water quality, and its toxicity could show carcinogenic consequences [8]. As a result, efficient and selective methyl orange detection and degradation methods are required [9].

For decades, a variety of techniques have been used to remove dye from industrial wastewaters, including reverse osmosis, reduction, segregation, coagulation, adsorption, oxidation, aerobic, micro and nanofiltration, ion exchange, anaerobic, flocculation, case structure, electrochemical, and photocatalytic degradation [10]. Due to the highly efficient, inexpensive, and ease of the dye degradation reaction in semiconductors including TiO<sub>2</sub>, SiO<sub>2</sub>, SnO<sub>2</sub>, WO<sub>3</sub>, ZnO, ZnS, Fe<sub>2</sub>O<sub>3</sub>, CdS, and others, photocatalytic degradation has been recognized as one of the most interesting techniques for removing organic dye from contaminated waters [11, 12]. Furthermore, by optimizing the photocatalyst component and surfaces with diverse nano-scale morphologies such as nanotubes, nanoparticles, nanofibers, dendrites, nanoplates, nanowires, and quantum dots, the photocatalytic degradation process may be enhanced [13, 14].

However, using semiconductor and transition-metal nanostructures for photocatalytic degradation of organic dyes has many benefits, no study has been done on the electrochemical and photocatalytic performance of Ag nanoparticles decorated on gallium arsenide films synthesized by electrodeposition method. Therefore, this study focused on the synthesis of Ag NPs/GaAs films through an electrodeposition method for considering the photocatalyst's properties for degradation of methyl orange (MO) dye.

## 2. MATERIALS AND METHODS

To eliminate native oxide on the surface of the GaAs wafers, they were cleaned with 10% HCl for 20 minutes. The GaAs samples were washed with enough deionized H<sub>2</sub>O before being dried with a flow of N<sub>2</sub>(g). After cooling the electrode, it was dipped in the electrochemical solution, and Ag nanoparticles were electrodeposited on GaAs using a mixture of 1M ascorbic acid (99%) and 0.5mM AgNO<sub>3</sub> (99%) in 0.1M phosphate buffer solution (PBS) at a scan rate of 10mV/s for 5 min. The Ag NPs/GaAs were washed and dried with Deionized water at room temperatures, respectively.

The morphology and microstructure of synthesized electrodes were evaluated using scanning electron microscopy (SEM) and X-ray diffraction (XRD) analysis. A 3900/U-3900H UV-VIS spectrophotometer (Hitachi, Ltd. Tokyo, Japan) was used to examine the optical absorption spectra of the produced specimens. EIS experiments were done in a typical three electrochemical system that included Pt rod, Ag/AgCl electrode, and prepared films as counter, reference, and working electrodes,

respectively, in a frequency range of 1000 mHz to 1 MHz at AC voltage of 5mV amplitude. The electrolyte used in the EIS test was 0.1M KCl (99%) with a 5mM  $[\text{Fe}(\text{CN})_6]^{3-/4-}$  (99%) solution.

Measurements of photodegradation were carried out in a test chamber containing a photocatalyst (Ag NPs/GaAs) and a 20mg/l methyl orange (MO) aquatic solution. A UV-VIS was used to measure the optical absorption spectra of produced films, with a UV Lamp (365nm) and a 300 W Xe Lamp used to irradiate UV and visible lights, respectively. After light irradiation, optical absorption spectra were collected, and the degradation efficiencies were calculated using the recorded absorption intensities of the degraded dye by using the equation:

$$\text{Degradation efficiency}(\%) = \left(1 - \frac{I_t}{I_0}\right) \times 100 = \left(1 - \frac{C_t}{C_0}\right) \times 100 \quad (1)$$

where  $I_0$  and  $C_0$  denote the absorption intensities and concentration of an undamaged MO solution, respectively. The absorption intensity and concentrations of irradiated MO solutions are represented by  $I_t$  and  $C_t$ , respectively. The effectiveness of the produced photocatalyst was also tested in wastewater collected from Nanjing, China's industrial wastewater. The samples were centrifuged at 2000 rpm, and the supernatant was utilized to make the 5 mg/MO solution as a real sample.

### 3. RESULTS AND DISCUSSION

Fig. 1 reveals the FESEM images of Ag nanoparticles on GaAs substrates. The average diameter of Ag NPs has obtained at 80nm. The FESEM image of Ag NPs/GaAs in Figure 1 displays a uniform distribution of silver nanoparticles on the surface of GaAs.

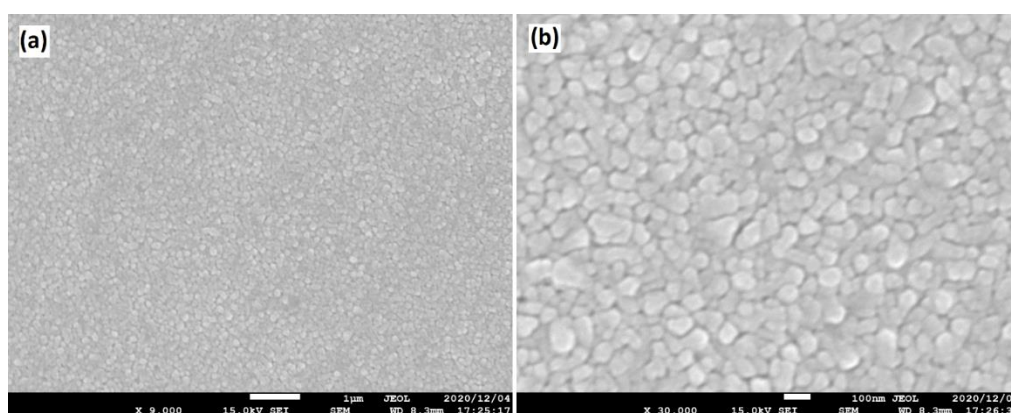


**Figure 1.** FESEM images of Ag nanoparticles on GaAs substrates

Diffraction peaks are obviously detected and are positioned in positions according to those predictable for GaAs, as shown by the JCPDS. The XRD patterns of Ag NPs/GaAs shows diffraction peaks at  $39.17^\circ$ ,  $44.22^\circ$ ,  $64.71^\circ$  and  $77.36^\circ$  that revealed to form (111), (200), (220) and (311) planes

of the Ag in fcc structures (JCPDS no. 04-0850), respectively [15]. Furthermore, the XRD pattern indicates both Ag NPs and GaAs diffraction peaks which reveals to effective deposition of AgNPs on GaAs substrate.

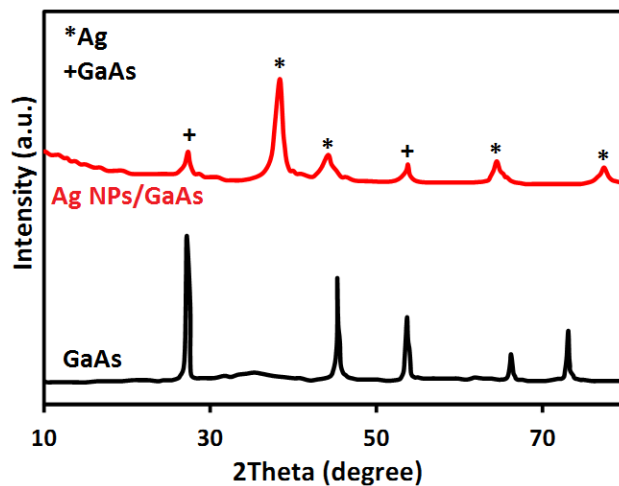


Figure 2. XRD pattern of (a) GaAs and Ag NPs/GaAs.

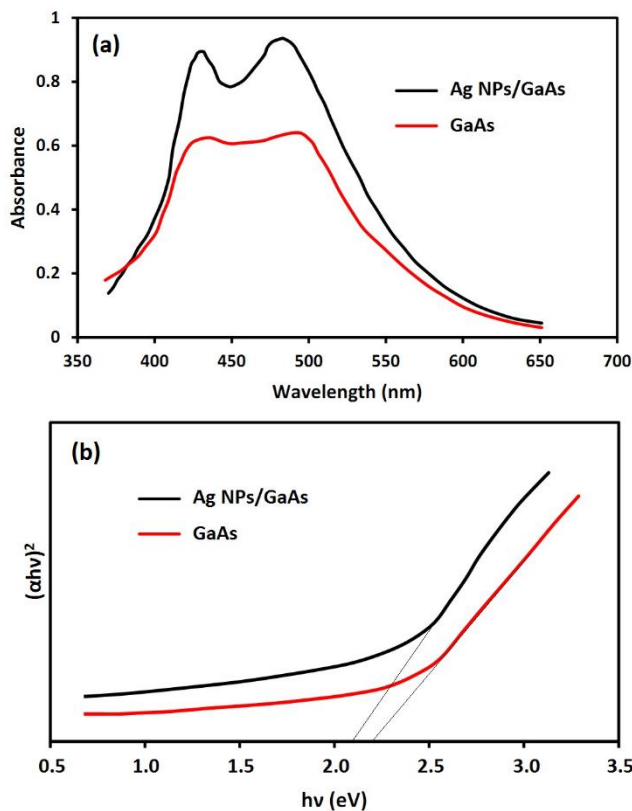


Figure 3. (a) Absorption spectrum and (b) Tauc curves of the GaAs and Ag NPs/GaAs in ambient temperature

Figure 3a shows the recorded absorption spectra of GaAs and Ag NPs/GaAs at room temperature. The redshift of the Ag NPs/GaAs film absorption edge toward GaAs film is seen, which might be attributed to the shrinking of the bandgap due to the existence of Ag levels in the GaAs energy gap.

This demonstrates that Ag NPs can extend the visible photoactivation range of GaAs films. Moreover, after coating with Ag NPs, the absorption increases, owing to the metal's greater absorption nature and the creation of a dipole activity state in the GaAs band-gap. The Tauc equation was used to calculate the optical band gap energy ( $E_g$ ) of the film, as follows [16]:

$$(\alpha h\nu)^{\frac{1}{2}} = A(h\nu - E_g) \quad (2)$$

Where  $\alpha$  indicates absorption coefficient,  $h$  reveals *Planck's constant* ( $4.1357 \times 10^{-15}$  eVs), and  $\nu$  presents the light frequency. The optical bandgap values for nanostructured GaAs and Ag NPs/GaAs films, as shown in Figure 3b, are 2.23 eV and 2.16 eV, respectively. The creation of oxygen vacancies during the coating process might increase the defect energy level just below the conduction band and move its edge in the forbidden gap, narrowing the bandgap [17].

The EIS analysis was conducted to consider the recombination and transfer of the charge at electrolyte and film and interfaces in 0.1M KCl inclosing 5mM  $[\text{Fe}(\text{CN})_6]^{3-/4-}$  solution in a frequency range of 1000 mHz to 1 MHz at AC voltage of 5mV amplitude. The Nyquist diagrams of EIS measurement of GaAs and Ag NPs/GaAs electrodes are displayed in Fig. 4. As can be seen, the Ag NPs/GaAs film has a shorter semicircle than the GaAs film, which is linked with greater interfacial charge transfer and a reduced photo-excited recombination rate due to efficient separation of photo-induced electron-hole pairs. These findings may be linked to a change in the conduction band, which reduces energy loss and enables photo-excited carriers [18].

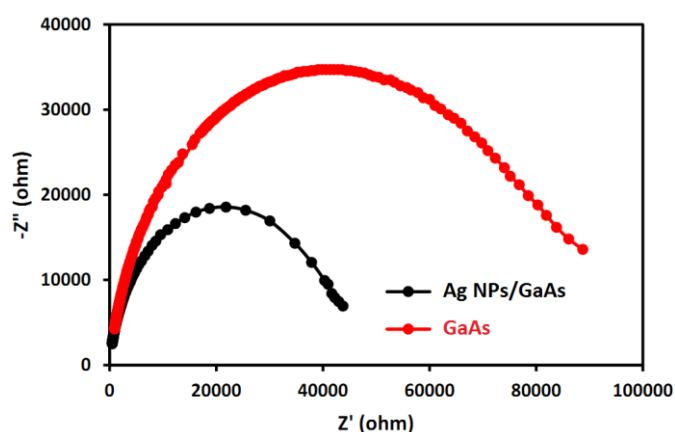


**Figure 4.** Nyquist diagrams of the GaAs and Ag NPs/GaAs electrodes in 0.1M KCl inclosing 5mM  $[\text{Fe}(\text{CN})_6]^{3-/4-}$  solution in a frequency range of 1000 mHz to 1 MHz at AC voltage of 5mV amplitude.

Figure 5 exhibits the degradation efficiency of 20mg/l of MO in the blank, GaAs, and Ag NPs/GaAs photocatalysts under-dark, visible and UV irradiations. As shown in Fig. 5a, degradation efficiency of 0.08 %, 1.42 %, and 1.74 % are attained after 20 minutes, and 0.16%, 1.59%, and 1.90% are obtained after 100min for blank, GaAs and Ag NPs/GaAs photocatalysts under dark conditions, respectively. Hence, the findings for dark circumstances show that poor deterioration (less than 1.5%) occurs in the first 20 minutes and that the rate of degradation is minor over the remaining 80 minutes. To reach adsorption-desorption equilibrium, the MO solutions were kept in the dark for 25 minutes before degradation experiments under UV and visible irradiation.

Moreover, the MO degradation efficiencies were 1.07 %, 36.7%, and 100% for blank, GaAs and Ag NPs/GaAs photocatalysts for 46 min UV irradiation, respectively (Figure 5b). The whole degradation of MO for GaAs photocatalyst was attained after 100 min of UV irradiation. Fig. 5c displays degradation efficiencies of 0.7%, 43.7%, and 100% were obtained for blank, GaAs and Ag NPs/GaAs photocatalysts for 40 min visible irradiation, respectively. Therefore, the degradation efficiency of GaAs film meaningfully is improved 64% and 36% by coating Ag NPs under UV and visible irradiations, respectively. The coating Ag NPs may change in GaAs electronic structure because of inducing oxygen-vacancies and development of novel energy levels in bandgap of GaAs that create active Ag NPs/GaAs under visible-light radiation [19, 20]. In the photocatalytic degradation of MO, the new energy levels increase electron-hole separation and enhance the density of contributing charges. GaAs has the lowest degradation rate in both ultraviolet and visible-light irradiations, owing to their small bandgap, which its greater electron-hole recombination rate reduces deterioration in the visible-light area. These findings are consistent with the work's optical and electrochemical investigations.

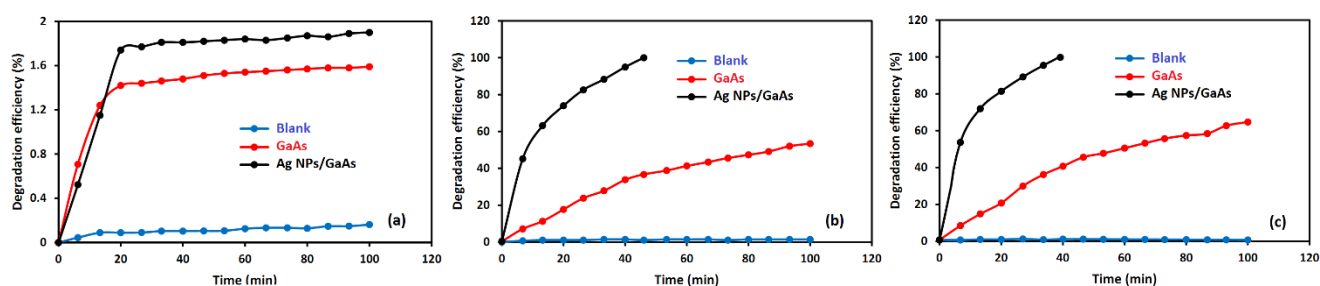


**Figure 5.** Degradation efficiencies of 20mg<sup>l</sup><sup>-1</sup> of MO in blank, GaAs and Ag NPs/GaAs photocatalysts under (a) dark condition (b) UV and (c) visible irradiations.

In Table 1, the results of this study were compared by other photocatalysts for MO degradation efficiency. This comparison indicates the high photocatalytic activities of Ag NPs/GaAs in the MO degradation under visible-irradiation, which may be contributed to the synergistic effects of porous structure, which facilitates the transfer of electrons in the Ag NPs/GaAs interface, cubic pyrite interface, and oxygen-vacancy, which can improve charge separation in the Ag NPs/GaAs interface [21].

Figure 6 shows UV–Vis spectra of photodegradation of 10mg/l MO produced from a real sample with regard to varied irradiation times by Ag NPs/GaAs photocatalyst. During the photodegradation events, the strength of the absorption peak at 470 nm constantly diminishes. In a real sample, the peak vanishes after 30 minutes of degradation. As a result, the study's novelty is the simple and low-cost preparation of Ag NPs/GaAs photocatalysis for treating MO from wastewaters under visible irradiation.

**Table 1.** The degradation efficiency of MO in prepared Ag NPs/GaAs photocatalysts compared to that of other photocatalysts.

Photocatalysts	MO content (mg/l)	Irradiation source	Degradation efficiency(%)	Degradation time(min)	Ref.
Ag NPs/GaAs	20.00	UV visible	100 100	46 40	This work
CaFe <sub>2</sub> O <sub>4</sub> /Fe <sub>2</sub> O <sub>3</sub>	20.00	visible	99	60	[22]
Sn-Fe bimetallic NPs	20.00	UV	95	35	[23]
Cu <sub>2</sub> O-modified ZnO nanorods	20.00	visible	85	100	[24]
BiVO <sub>4</sub> /Bi <sub>2</sub> S <sub>3</sub> /MoS <sub>2</sub> heterojunction	20.00	visible	94	300	[25]
Ag/TiO <sub>2</sub> nanocomposites	20.00	visible	65	120	[26]
Ag <sub>3</sub> PO <sub>4</sub> /TiO <sub>2</sub> heterostructure	20.00	visible	95	60	[27]

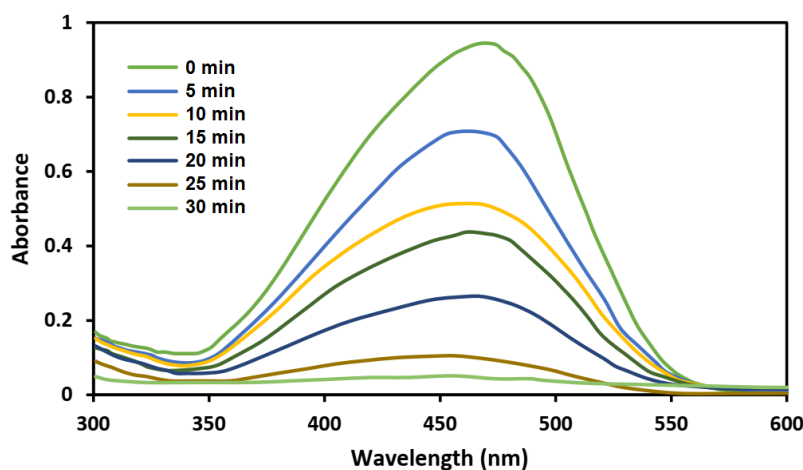


**Figure 6.** UV–Vis spectrum of photocatalytic degradation process of 10mg/l MO made from real sample at various irradiation times with Ag NPs/GaAs photocatalyst.

#### 4. CONCLUSIONS

In this study, the Ag nanoparticles were decorated on a GaAs electrode by electrodeposition method and their use as photocatalysts for the degradation of MO dyes under UV and visible

irradiation were investigated. SEM and XRD were used to examine the morphology and structure of the produced electrodes, revealing that Ag NPs in fcc structures were electrodeposited uniformly on the GaAs electrode surface. According to the optical studies, the optical band-gap values for nanostructured GaAs and Ag NPs/GaAs films were 2.23 eV and 2.16 eV, respectively. According to EIS analysis, the Ag NPs/GaAs film had a decreased photo-excited carrier recombination rate due to the effective separation of photo-induced electron-hole pairs. MO photodegradation experiments demonstrate that under UV and visible radiation, complete elimination of MO takes 46 and 40 minutes, respectively. As a result of lowering optical bandgaps, photocatalytic activity on Ag NPs/GaAs photocatalyst was significantly enhanced under visible light.

#### ACKNOWLEDGEMENT

This research was supported by the Science and Technology Project of Henan Province 212102210217 and Key scientific research project of higher education of Education Department Henan Province 21A140019.

#### References

1. R. Raman, *GM crops & food*, 8 (2017) 195.
2. P.H. Raven and D.L. Wagner, *Proceedings of the National Academy of Sciences*, 118 (2021) 1.
3. Y. Orooji, B. Tanhaei, A. Ayati, S.H. Tabrizi, M. Alizadeh, F.F. Bamoharram, F. Karimi, S. Salmanpour, J. Rouhi and S. Afshar, *Chemosphere*, 281 (2021) 130795.
4. C.E. Scruggs and C.M. Heyne, *Wiley Interdisciplinary Reviews: Water*, 8 (2021) e1543.
5. B. Maryam and H. Büyükgüngör, *Journal of Water Process Engineering*, 30 (2019) 100501.
6. N. Sarwar, U.B. Humayoun, M. Kumar, S.F.A. Zaidi, J.H. Yoo, N. Ali, D.I. Jeong, J.H. Lee and D.H. Yoon, *Journal of Cleaner Production*, 292 (2021) 125974.
7. Y. Orooji, P.N. Asrami, H. Beitollahi, S. Tajik, M. Alizadeh, S. Salmanpour, M. Baghayeri, J. Rouhi, A.L. Sanati and F. Karimi, *Journal of Food Measurement and Characterization*, (2021) 1.
8. N.E.-A. El-Naggar, R.A. Hamouda, A.A. Saddiq and M.H. Alkinani, *Scientific Reports*, 11 (2021) 1.
9. Y. Liang, Y. Yang, C. Zou, K. Xu, X. Luo, T. Luo, J. Li, Q. Yang, P. Shi and C. Yuan, *Journal of Alloys and Compounds*, 783 (2019) 848.
10. P.S. Kumar, G.J. Joshiba, C.C. Femina, P. Varshini, S. Priyadharshini, M.A. Karthick and R. Jothirani, *Desalin. Water Treat.*, 172 (2019) 395.
11. A. Manikandan, E. Manikandan, S. Vadivel, M. Kumaravel, D. Maruthamani and S. Hariganesh, *Organic Pollutants in Wastewater I*, 45 (2018) 183.
12. L.L. Mphahlele and P.A. Ajibade, *International Journal of Electrochemical Science*, 15 (2020) 1206.
13. D. Tan, H. Long, H. Zhou, Y. Deng, E. Liu, S. Wang and S. Zhang, *International Journal of Electrochemical Science*, 15 (2020) 12232.
14. H. Karimi-Maleh, Y. Orooji, F. Karimi, M. Alizadeh, M. Baghayeri, J. Rouhi, S. Tajik, H. Beitollahi, S. Agarwal and V.K. Gupta, *Biosensors and Bioelectronics*, 184 (2021) 113252.
15. R. Kalavani, M. Maruthupandy, T. Muneeswaran, A.H. Beevi, M. Anand, C. Ramakritinan and A. Kumaraguru, *Frontiers in Laboratory Medicine*, 2 (2018) 30.
16. Ö.B. Mergen and E. Arda, *Synthetic Metals*, 269 (2020) 116539.
17. L. Dong, R. Jia, B. Xin, B. Peng and Y. Zhang, *Scientific reports*, 7 (2017) 1.

18. S. Saha, A. Victorious and L. Soleymani, *Electrochimica Acta*, 380 (2021) 138154.
19. Q. Chu, J. Li, S. Jin, S. Guo, E. Park, J. Wang, L. Chen and Y.M. Jung, *Nanomaterials*, 11 (2021) 1292.
20. H. Karimi-Maleh, M.L. Yola, N. Atar, Y. Orooji, F. Karimi, P.S. Kumar, J. Rouhi and M. Baghayeri, *Journal of colloid and interface science*, 592 (2021) 174.
21. C. Ling, X. Liu, M. Li, X. Wang, Y. Shi, J. Qi, J. Zhao and L. Zhang, *Applied Catalysis B: Environmental*, 290 (2021) 120051.
22. Y. Fu, S. Shan, F. Chen and J. Hu, *Journal of Materials Science: Materials in Electronics*, 31 (2020) 17967.
23. A. Bahadoran, Q. Liu, B. Liu, J. Gu, D. Zhang, A. Fakhri and V.K. Gupta, *Spectrochimica Acta Part A: Molecular and Biomolecular Spectroscopy*, 253 (2021) 119592.
24. X. Jiang, Q. Lin, M. Zhang, G. He and Z. Sun, *Nanoscale research letters*, 10 (2015) 1.
25. J. Wang, J. Jin, X. Wang, S. Yang, Y. Zhao, Y. Wu, S. Dong, J. Sun and J. Sun, *Journal of colloid and interface science*, 505 (2017) 805.
26. X. Zheng, D. Zhang, Y. Gao, Y. Wu, Q. Liu and X. Zhu, *Inorganic Chemistry Communications*, 110 (2019) 107589.
27. H. Liu, D. Li, X. Yang and H. Li, *Materials Technology*, 34 (2019) 192.

© 2022 The Authors. Published by ESG ([www.electrochemsci.org](http://www.electrochemsci.org)). This article is an open access article distributed under the terms and conditions of the Creative Commons Attribution license (<http://creativecommons.org/licenses/by/4.0/>).